**SCIENCE CHINA**
Information Sciences

• **Supplementary File** •

# Terahertz magneto-optical isolator based on graphene-silicon waveguide

Dan ZHAO[1], Fei FAN[1*], Tengfei LI[1], Zhiyu TAN[2], Jierong CHENG[2] & Shengjiang CHANG[3]

[1]*Institute of Modern Optics, Nankai University, Tianjin Key Laboratory of Micro-scale Optical Information Science and Technology, Tianjin* 300350, *China;*
[2]*Tianjin Key Laboratory of Optoelectronic Sensor and Sensing Network Technology, Tianjin* 300350, *China*

## Appendix A THz magneto-optical properties of graphene

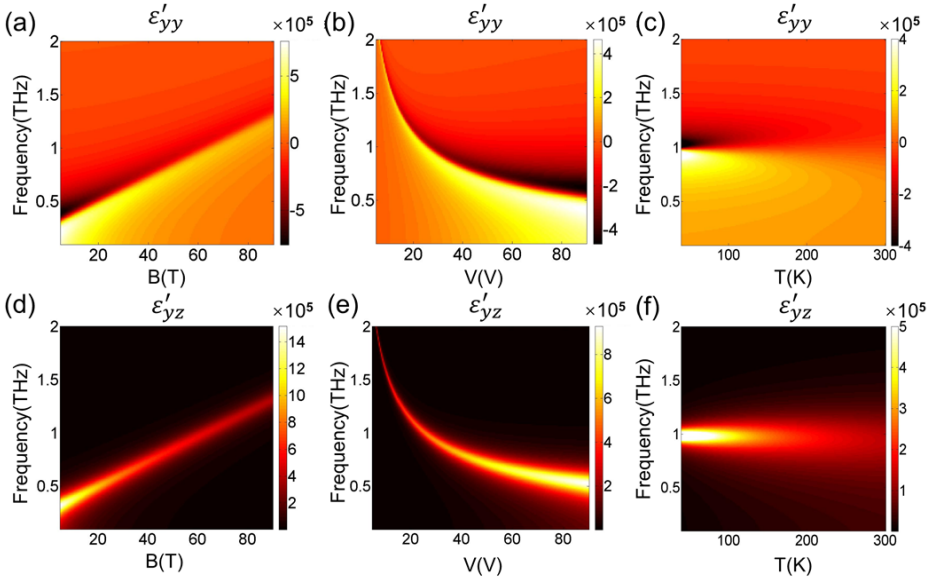


**Figure A1** The dielectric function map of graphene v.s frequency and external field. The map of the real part of $\varepsilon_{yy}$ changes with (a) the different biased magnetic field at 60 V, 80 K; (b) the different biased voltage at 2 T, 80 K; (c) the different temperature at 2 T, 60 V. The map of the real part of $\varepsilon_{yz}$ changes with (d) the different biased magnetic field at 60 V, 80 K; (e) the different biased voltage at 2 T, 80 K; (f) the different temperature at 2 T, 60 V.

With the external magnetic field along the $x$-direction, the dielectric function of graphene is a non-reciprocal tensor, as shown Eq. (A1) [1-3]:

$$\begin{bmatrix} \varepsilon_{xx} & 0 & 0 \\ 0 & \varepsilon_{yy} & \varepsilon_{yz} \\ 0 & \varepsilon_{zy} & \varepsilon_{zz} \end{bmatrix} \tag{A1}$$

In Eq. (A1), three different tensor elements can be expressed as :

$$\varepsilon_{yy} = \varepsilon_{zz} = 1 - \frac{2D}{\pi\varepsilon_0 t}\frac{\omega + i\gamma}{\omega\left[(\omega + i\gamma)^2 - \omega_c^2\right]} \tag{A2}$$

$$\varepsilon_{yz} = -\varepsilon_{zy} = 1 + \frac{2D}{\pi\varepsilon_0 t}\frac{i\omega_c}{\omega\left[(\omega + i\gamma)^2 - \omega_c^2\right]} \tag{A3}$$

* Corresponding author (email: fanfei@nankai.edu.cn)

$$\varepsilon_{xx} = 1 + \frac{2D}{\pi\varepsilon_0 t}\frac{1}{\omega(\omega + i\gamma)} \tag{A4}$$

where $v_F$ is Fermi velocity and $v_F \approx 10^6$m/s; $D = e^2E_F/2\hbar^2$is the weight of Drude model; $\omega_c = eBv_F^2/E_F$ is cyclotron frequency; $E_F = hv_F\sqrt{\pi N}$ is Fermi level; $N = 7.2 \times 10^{14}V(\mathrm{m}^{-2})$ is carrier concentration; $V$ is the biased voltage of the external electric field on the graphene surface; $\tau = 1/\gamma = \mu E_F/ev_F^2$ is the relaxation time; $\mu = 10^{10}/\left[19^2\left(N/10^{12}\right)T\right]$ $(\mathrm{m}^2\mathrm{V}^{-1}\mathrm{s}^{-1})$ is carrier mobility; $\varepsilon_0$ is the vacuum permittivity and the permittivity of Si is 11.7 [4-9].

It can be seen from the above expressions that the electromagnetic tensor elements of graphene are dependent on the external magnetic field, electric field, and temperature. Fig.A1. shows the real part of $\varepsilon_{yy}$ and $\varepsilon_{yz}$ map of graphene with different external magnetic fields, the biased voltages, and temperature calculated by Eqs. (A2) and (A3), respectively. They show the pattern of the Lorentz spectrum line. There is a sharp cyclotron resonance with a strong dispersion near $\omega_c$, and the resonant frequency proportionally increases with the increase of the external magnetic field as shown in Fig. A1(a), A1(d). On the contrary, with the increase of the external electric field, the resonant frequency of the dielectric constant decreases. With the increase of voltage, the change tends to be flat. Near the cyclotron resonance, graphene exhibits a strong non-reciprocal magneto-optical effect, which strongly changes the polarization state of the incident electromagnetic wave.

## Appendix B Non-reciprocal polarization conversion in the graphene-Si waveguide

As shown in Fig.1(a) of the main text, the graphene layer is attached to one side of the waveguide structure, and $B$ is along the $x$-direction and perpendicular to the graphene layer, so the waveguide structure is asymmetric. The substrate material is $SiO_2$, and the waveguide material is Si. The optimized waveguide geometry is respectively that $a = 40$ $\mu$m, $b = 60.9$ $\mu$m, $L = 600$ $\mu$m. The height of graphene $h = 25.8$ $\mu$m and the graphene's thickness $\Delta = 1$ nm.The height of the $SiO_2$ substrate $H = 30$ $\mu$m and the width is $W = 140$ $\mu$m.

We used COMSOL Multiphysics to simulate the field distributions for the forward transmission and backward transmission in the condition of $B = 2$ T, $V = 60$ V, and $T = 80$ K, as shown in Fig.B1. As shown in Figs. B1(a) and B1(b), if the coordinate system is established always along the direction of light propagation, the waveguide structures for forward and backward propagation are opposite to the direction of the biased magnetic field. Since the non-reciprocal tensor of graphene under the biased magnetic field, this asymmetric waveguide structure can achieve non-reciprocal transmission [10]. In this waveguide, the fundamental modes are no longer the strict TE and TM modes, in fact, they are both hybrid polarization modes. The fundamental modes of the forward and backward transmission are shown in Fig. B1(c) and B1(d), respectively, they are quite different: the electric field of the forward wave goes along the $y$-direction (Longitudinal mode), and the backward goes along the $x$-direction (Transverse mode). The effective refractive index curves of fundamental modes are also drawn in Fig. B1(e). There is a big gap between the real and imaginary parts of the forward and backward effective refractive index in the frequency range of 1.2 - 1.8 THz. The eigenmode analysis above shows that this magneto-optical waveguide supports different orthogonal polarization modes in the forward and backward transmission, which is the theoretical basis for the realization of non-reciprocal transmission.

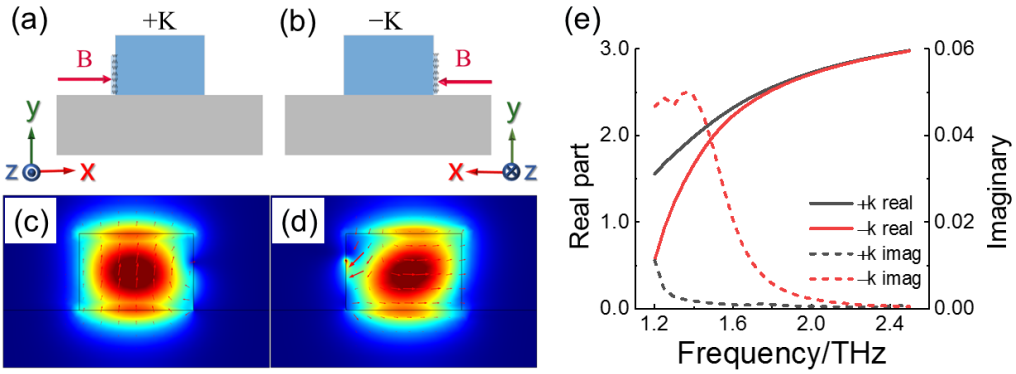


**Figure B1** Eigenmode analysis of graphene-Si waveguide at $B = 2$ T, $V = 60$ V, and $T = 80$ K. The cross-section structure of waveguide for (a) forward (+K) and (b) backward transmission (-K). Fundamental mode pattern of (c) forward (+K) and (d) backward transmission (-K). (e) The real and imaginary part of fundamental modes' effective refractive index for the forward and backward transmission.

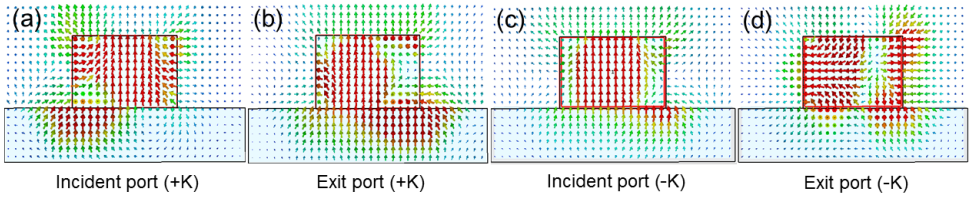


**Figure B2** The electric field patterns of incident and exit ports for the forward and backward transmission.

Further, the mode field distribution of the forward and backward waves at the input and output ports are shown in Fig. B2. For forward transmission, its fundamental mode is just the longitudinal mode along $y$-axis shown in Fig. B1(c), so the input

$y$-polarization mode keeps the original polarization state in the waveguide and weak magneto-optical interaction with graphene layer. Finally, a longitudinal linear polarization output can be detected. For backward transmission, its fundamental mode is the transverse mode along $x$-axis, and the input $y$-polarization is gradually converted into transverse mode at the output port under the magneto-optical polarization conversion effect of graphene, so the detector will not detect the $y$-polarization component of the backward wave at the output port. Therefore, the one-way transmission in this waveguide is essentially due to the non-reciprocal polarization conversion effect in the waveguide.

## Appendix C Isolator based on graphene-Si waveguide and resonant ring

The resonant ring isolator is shown in Fig. C1. The structure materials used are the same as graphene-Si waveguide structure. The optimized waveguide geometry is that $a = 40$ $\mu$m, $b = 60.9$ $\mu$m, $z = 25.8$ $\mu$m, and $L_1 = 1000$ $\mu$m. The length of the straight waveguide in the resonant ring $L' = 80$ $\mu$m. The ex-radius of the resonant ring is $R = 95.9$ $\mu$m. The distance between the graphene-Si waveguide and ring $\Delta_1 = 1$ $\mu$m. The graphene's thickness $\Delta = 1$ nm.

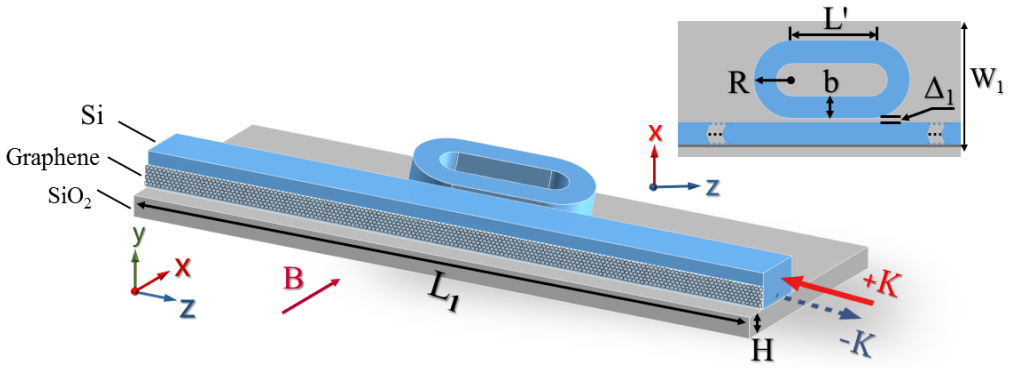


**Figure C1** Geometry of the resonant ring isolator structure.

Fig. C2 shows the tunability of this device with the external magnetic field and electric field. In the case of $T = 80$ K, the isolation spectral lines are shown in Figs. C2(a) and C2(b) with different magnetic fields ($B = 0$ - 2.4 T) and different voltages ($V = 50$ - 100 V). When $B = 0$ T, the resonant ring isolator does not have non-reciprocal transmission. When $B = 2$ T, $V = 60$ V, the isolation effect and operating bandwidth are close to the best. The insertion loss spectrum lines are also shown in Figs. C2(c) and C2(d) under different magnetic fields and different bias voltages, respectively. For the case of 2 T and 60 V, the insertion loss is 8 dB within the 10 dB-work bandwidth range, and the lowest insertion loss is 5 dB at 1.48 THz. This insertion loss is still within an acceptable order for a THz waveguide device.

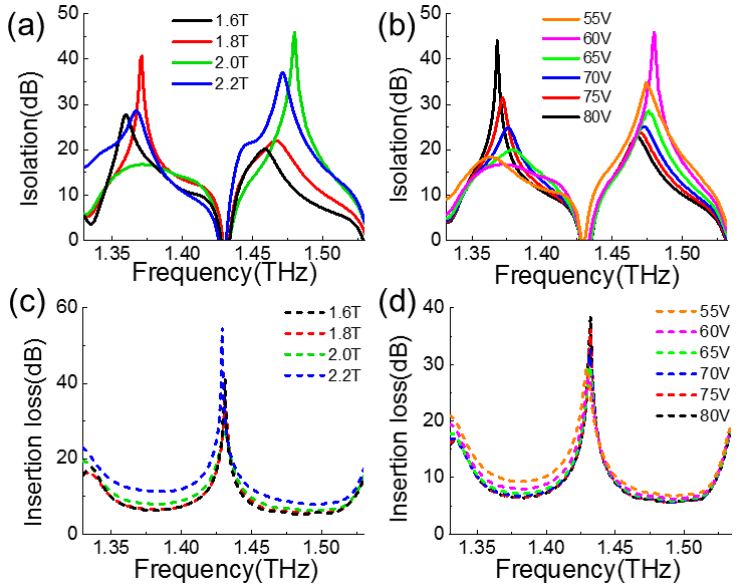


**Figure C2** Tunability analysis of the resonant ring isolator. Isolation spectrum (a) under the different magnetic fields at $V = 60$ V and (b) the different voltages at $B = 2$ T. Insertion loss spectrum (c) under the different magnetic fields at $V = 60$ V and (d) the different voltages at $B = 2$ T.

## Appendix D Four-port isolator

Finally, a four-port isolator is demonstrated shown in Fig. D1. To reduce the bend loss of THz wave in the resonant ring, the radius of the ring is increased. The optimized straight waveguide geometry is that $a = 40$ $\mu$m, $b' = 60$ $\mu$m, and $L_1 = 1000$ $\mu$m. The height of graphene $h' = 26$ $\mu$m, the inner diameter $r = 264.3$ $\mu$m, and straight waveguide length $L_2 = 143.4$ $\mu$m. The distance between the straight waveguides and the resonant ring is $\Delta_1 = 1$ $\mu$m. According to Eqs A(2), A(3) and their auxiliary parameters, we can see that the THz optical and magneto-optical properties of graphene are also related to temperature. In Appendix B and Appendix C, the devices are designed at 80 K. Considering that the devices operating at the room temperature of 300 K are more practical, for this four-port one-way transmission device, we show that the possibility of such graphene magneto-optical devices working at the room temperature of 300 K. In the following discussion, $B = 0.9$ T, $V = 10$ V and $T = 300$ K.

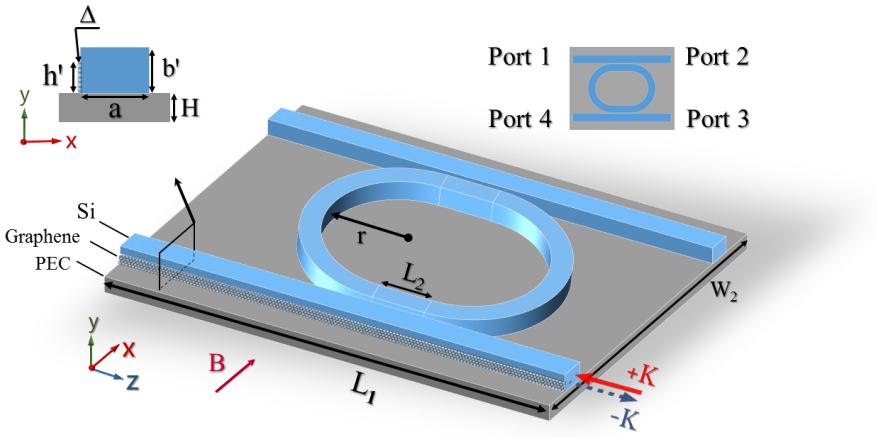


**Figure D1** Geometry detail of the proposed four-port isolator structure

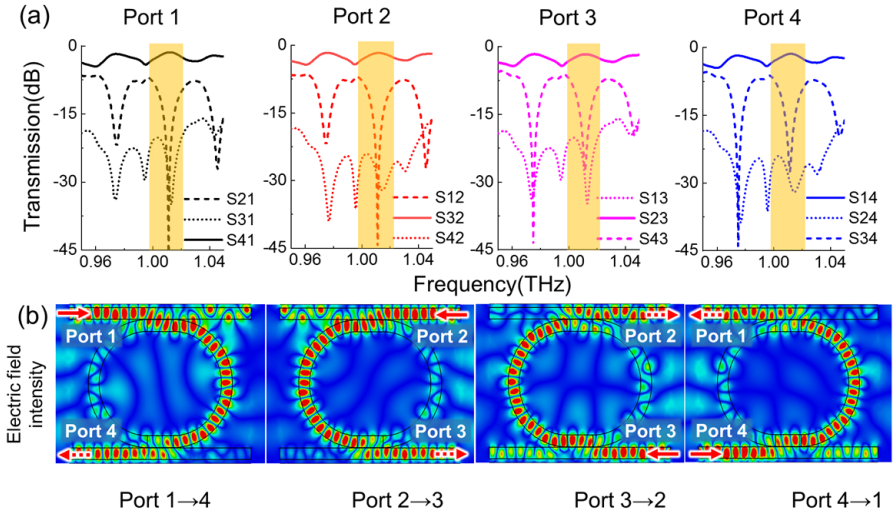


**Figure D2** Transmission spectrum and (b) electric field patterns when light incidences from Port 1, 2, 3, 4 at $B = 0$ T, $V = 10$ V, $T = 300$ K.

When $B = 0$ T, the transmission spectrum of each port is shown in Fig. D2. The transmission curves with high transmittance are displayed by the solid lines, the transmission curves with low transmittance are shown with the dashed lines, and the working bandwidth is highlighted in the yellow color in Fig. D2(a). Without the biased magnetic field, graphene's nonreciprocity disappears, so the device only acts as a ring resonator. Fig. D2(b) shows the electric field distribution of incident waves from Port 1, 2, 3, and 4 at $f = 1$ THz. The main propagation path is Port 1→4, Port 4→1 and Port 2→3, Port 3→2. In other ports, there is almost no wave output, so the transmission is reciprocal when there is no biased magnetic field.

When $B = 0.9$ T (along the positive direction) and - 0.9 T (along the reverse direction), the graphene layer shows the magneto-optical effect. The transmission spectral lines of each port are shown in Fig. D3. The electric field distributions are presented below in Fig. D4 to better display the functions of the four-port isolator. As shown in Fig. D3(a), when the wave inputs from Port 4, the wave can forward transmit through the graphene-Si waveguide, and exit from Port 1 by coupling with the resonant ring. When the light inputs from Port 1, it couples into graphene-Si waveguide structure through the resonant ring. In this case, the light travels along the backward direction of the graphene-Si waveguide structure, so the light cannot exit from Port 4. Therefore, most of the waves transmit along with the straight waveguide structure and exit from Port 2. When the light inputs from Port 2, it couples with the resonant ring to the graphene-Si waveguide and can forward transmit and exit from Port 3. When the light inputs from Port 3, it travels along the backward direction of the graphene-Si waveguide. The light cannot enter the waveguide, so

Port 3 is closed. In general, in this four-port isolator, the transmission cycle is Port 4→1→2→3→× when $B$ = 0.9 T. The reverse cycle of the four-port isolator (Port 3→2→1→4→×) can also be explained in the same way when $B$ = - 0.9 T as shown in Fig. D3(b). Therefore, this device realizes nonreciprocal one-way transmission. But it is different from the traditional circulator, which can't realize one-way transmission in a cycle (Port 1→2→3→4→1), so we still call it isolator.

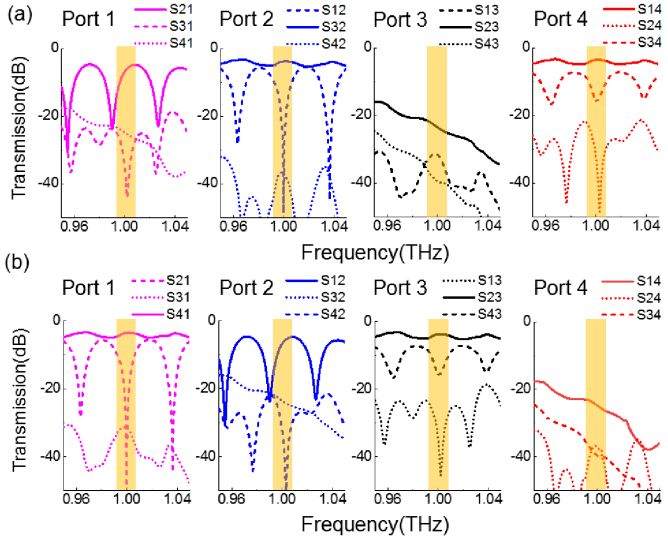


**Figure D3** The transmission spectrum when light incidences from Port 1, 2, 3, 4 at $f$ = 1 THz when (a) $B$ = 0.9 T and (b) $B$ = - 0.9 T.

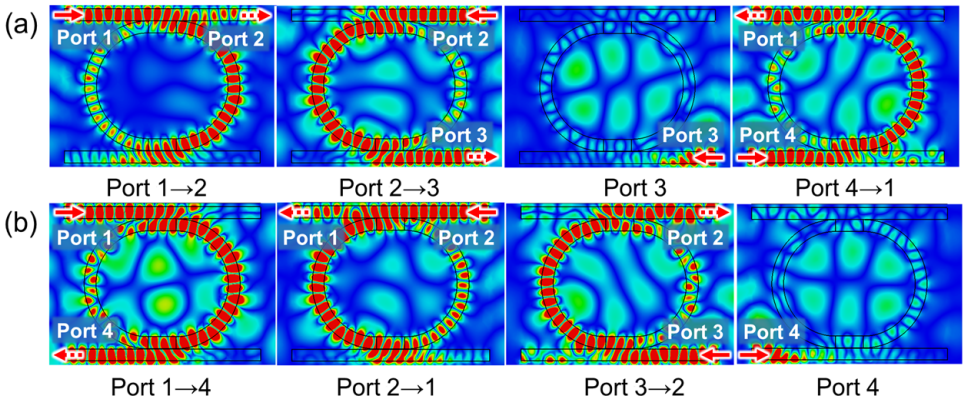


**Figure D4** The electric field patterns when light incidences from port 1,2,3,4 at $f$ = 1 THz when (a) $B$ = 0.9 T and (b) $B$ = - 0.9 T.

**References**


1 Yao X, Tokman M, et al. Efficient Nonlinear Generation of THz Plasmons in Graphene and Topological Insulators. Physical Review Letters, 2014, 112: 055501
2 Vakil A, Engheta N. Transformation Optics Using Graphene. Science, 2011, 332: 1291-1294
3 Poumirol J M, Liu P, et al. Magneto-plasmonic terahertz resonances in patterned graphene metasurfaces. APS March Meeting 2017. American Physical Society, 2017, 910-914
4 Padmanabhan P, Boubanga-Tombet S, et al. A graphene-based magnetoplasmonic metasurface for actively tunable transmission and polarization rotation at terahertz frequencies. Applied Physics Letters, 2020, 116: 221107
5 Tymchenko M, Nikitin A Y, et al. Faraday Rotation Due to Excitation of Magnetoplasmons in Graphene Microribbons. ACS Nano, 2013, 7: 9780-7
6 Crassee I, Orlita M, et al. Intrinsic Terahertz Plasmons and Magnetoplasmons in Large Scale Monolayer Graphene. Nano Letters, 2012, 12: 2470-2474
7 Qin J, Xia S, et al. Enhanced Faraday rotation and magneto-optical figure of merit in gold grating/graphene/silicon hybrid magneto-plasmonic devices. APL Photonics, 3: 016103
8 Guo J, Dai X, et al. Excitation of graphene magneto-plasmons in terahertz range and giant Kerr rotation. Journal of Applied Physics, 2019, 125: 013102
9 Bonaccorso F, Sun Z, et al. Graphene photonics and optoelectronics. Nature Photonics, 2010, 4: 611-622

10 Fan F, Chen S, et al. A review of magneto-optical microstructure devices at terahertz frequencies, IEEE Journal of Selected Topics in Quantum Electronics, 23: 8500111.